

A miniaturised 3-D Particle-Tracking Velocimetry System to measure the Pore Flow within a Gravel Layer

Michael Klar, Peter Stybalkowski, Hagen Spies, Bernd Jähne

Interdisciplinary Center for Scientific Computing
Digital Image Processing Research Group
University of Heidelberg
Im Neuenheimer Feld 368
69120 Heidelberg
Germany
e-mail: Michael.Klar@iwr.uni-heidelberg.de

ABSTRACT

This paper introduces a novel experimental setup that enables 3-D particle-tracking velocimetry (3-D PTV) measurements of the turbulent pore flow within a single pore of a gravel layer. The core of this setup is an artificial pore made up of pebbles fixed to each other, see Figure 1. Optical access to the pore volume is given by two flexible endoscopes, so-called *bendoscopes*. The artificial pore is embedded in a gravel bed at the bottom of an open-channel flow. Tracer particles are added to visualise the pore flow, and standard CCD-cameras are used to acquire digital image sequences of the flow field inside the artificial pore. Analysis of the image sequences by digital image processing techniques, namely a 3-D PTV algorithm, yields the Lagrangian flow velocities of the tracer particles along their trajectories, see Figure 2. The algorithm is based on stereo correlation of the particle trajectories; the 3-D coordinates are calculated by triangulation of corresponding optical rays. Correlating 2-D trajectories instead of the positions of single particles allows for a simple setup with a minimum number of two cameras resp. endoscopes. Extensive flow measurements under different flow conditions have been carried out in an experimental flume located at the Federal Waterways Engineering and Research Institute (Bundesanstalt für Wasserbau, BAW) in Karlsruhe, Germany. The impact of the turbulent free surface flow on the pore flow inside the gravel bed is clearly reflected in the measurement results. In the conducted experiments, fluctuations of pore velocity are mainly driven by surface waves in the open-channel flow. The results of the velocity estimates have been verified by simultaneous measurements of the free surface flow velocity and of pressure fluctuations. These studies are part of an international research project with the objective to quantify the influence of turbulent velocity and pressure fluctuations on the stability of river beds. It could be shown, that the presented setup is well suited for this task, and it will be extended and used for further research in this area.

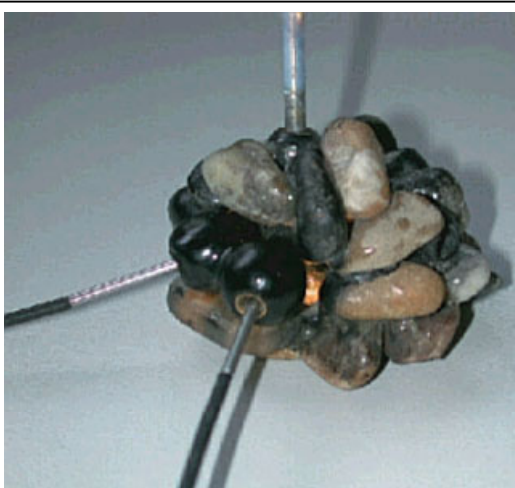


Fig. 1. The artificial pore with the two bendoscopes and the illumination fibre. The bendoscopes are attached to the pore in a stereo rig enabling 3-D flow measurements.

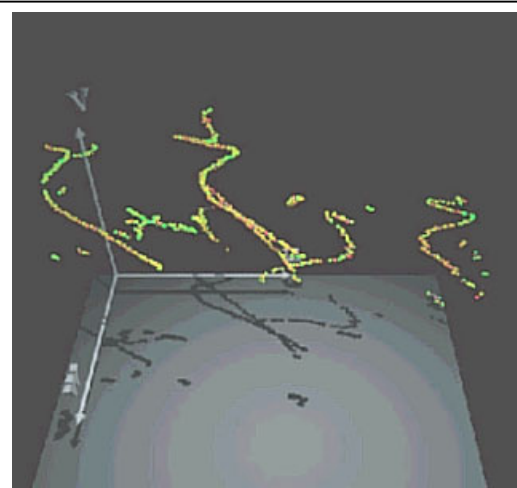


Fig. 2. Reconstructed 3-D Lagrangian particle trajectories within the pore volume. Velocities are encoded in colors: green=low, yellow=medium, red=high.

1. INTRODUCTION AND PURPOSE

The physical processes that drive the entrainment, transport and deposition of sediment grains, both in turbulent boundary layers and flows in porous media, are of considerable importance to a number of environmental sciences, including sedimentology, oceanography, geomorphology and fluid mechanics (Pye, 1994). This field of research is not only of academic interest, but it is also significant to environmental problems and hydraulic engineering tasks.

A major topic in fluvial hydraulics is *incipient* sediment transport, i.e. the question of bed stability of natural rivers and waterways. More precisely, this addresses the problem of the stability of gravel grains at the interface of the turbulent free surface flow above and the pore flow within the gravel layer of a river bed. A number of (semi-)empirical models for (incipient) sediment transport have been proposed (e.g. Yalin, 1977, 1992, Thorne et al., 1987). In hydraulic engineering applications, so-called Shields-curves, based on the original work of A. Shields (Shields, 1936), are used to determine river bed stability. Knowing the mean parameters of the fluid and the sediment material, one can determine the critical bed shear stress for the initiation of sediment transport from the Shields-curves and thus estimate the stability of the river bed. However, stability estimation from Shields curves doesn't yield reliable results in all cases, since the Shields curves are based on mean flow and grain properties and are strictly valid only under idealised laboratory conditions, e.g. stationary flow, homogeneous bed roughness, straight channels. Real flows almost always show a different behaviour. Both the bed geometry (e.g. gravel size distribution, bedforms and bed impurities, ripples, dunes) and the flow structures (e.g. secondary currents, separation flows, coherent motions, turbulence) are characterised by highly stochastic variations in space and time. Most of the existing approaches to sediment threshold don't incorporate the structures and pronounced dynamics of fluvial flows in an appropriate way.

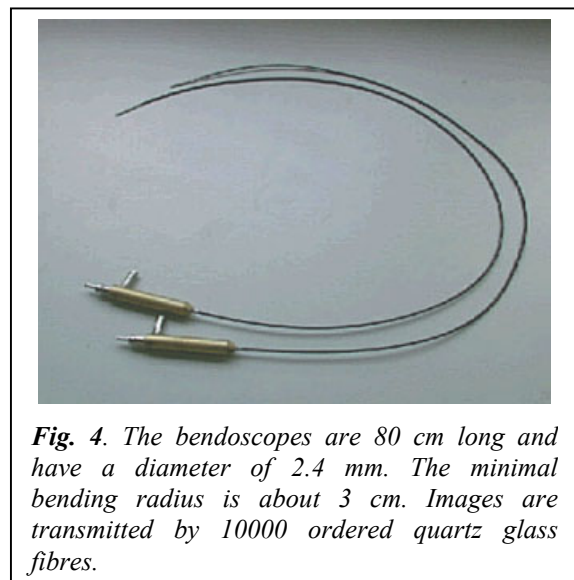
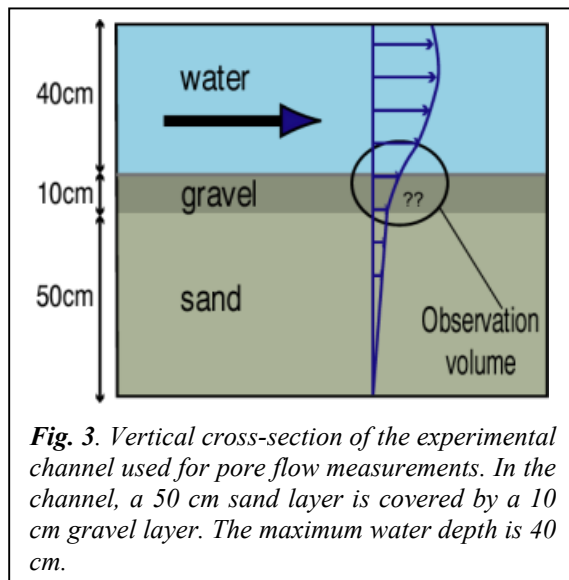
The most prominent features that have to be considered in the determination of river bed stability are the strong fluctuations of pressure and velocity in the turbulent flow field in and above the river bed (Nezu and Nakagawa, 1993, Yalin, 1977). Flow velocity, dynamic pressure and the induced hydrodynamic shear and lift forces are all strongly fluctuating quantities. Their extremal values can exceed the corresponding mean values significantly. The turbulent fluctuations are the result of a complex interaction between the free surface flow, the pore flow and the dynamic flow structures near the bed. The latter comprise vortex layers separating from roughness elements and the well-known near-wall coherent structures (Kline et al., 1967, Grass, 1971, Grass et al., 1996). Many authors point out the importance of (coherent) turbulent flow structures near the bed on the entrainment of sediment particles (e.g. Dittrich, 1997, Garcia et al., 1995, Dancy et al., 2000, Sechet, P. and Le Guennec, B., 1999). Different approaches to determine hydrodynamic lift and shear forces on single grains (e.g. Dittrich et al., 1996, Dey et al., 1999) include the effects of turbulent fluctuations into the calculations. However, there is still no universal, physically well-founded concept to answer the questions of river bed destabilisation. The fundamental knowledge of much of the sediment physics remains relatively primitive. Single sediment processes like erosion, sedimentation or fluidisation are not understood well enough to enable a general prediction of river bed stability. This lack of fundamental physical knowledge is due to the great complexity of the topic. In particular, experimental data are quite rare due to the difficult experimental conditions, both in laboratory flows and in the field (e.g. Clifford et al., 1993). A more detailed investigation of the fundamental physical processes governing the flow and pressure fields in the vicinity of river beds is a necessary first step towards improved and more reliable design formulae for engineering practice. Obviously, these processes take place in the boundary layer between the free surface flow and the pore flow. In the case of a base layer of fine (sand) bed material covered by a layer of coarser pebbles – which is the relevant situation for the design of bed and bank protection works in hydraulic engineering, compare the experimental configuration in Figure 3 – there is a second boundary layer at the interface between the coarse and fine materials. The two boundary layers are linked by the pore flow, which is in turn driven by the free surface flow. Thus, research concerning bed stability and sediment transport, or, more general, concerning exchange of mass and momentum between river bed and bulk flow, has to focus on the pore flow, the corresponding boundary layers and their mutual interaction.

In order to gain more insight into the highly dynamic (turbulent) flow fields in and above the porous medium of a river bed, in particular into their interaction and their impact on sediment entrainment, the presented measurement setup has been designed. This novel setup enables temporally and spatially highly resolved 3-D velocity measurements inside a single pore volume. The presented experimental studies are part of an international research project with the objective to quantify the impact of turbulent velocity and pressure fluctuations on the stability of river beds. In the experiments carried out at the Federal Waterways Engineering and Research Institute (Bundesanstalt für Wasserbau, BAW) in Karlsruhe, Germany, the fluctuating flow and pressure fields in and above a gravel layer in an open-channel flow are recorded. One of the major interests of these investigations is to quantify the influence of the turbulent free surface flow on the pore flow, e.g. the penetration of turbulent fluctuations into the gravel layer as a function of the vertical coordinate. Extreme values of these fluctuations are considered to be responsible for bed destabilisation.

The motivation of these experiments is twofold. First, more extensive experimental data helps to understand the basic phenomena and to develop modified theoretical approaches describing bed stability. Second, the data can be used to validate large eddy simulations of the flow field in and above a porous medium by comparing the statistical mean values of experiment and simulation. The numerical simulation of such a flow enables the calculation of instationary local velocity and pressure fields (Lang et al., 2001). The latter can be used to directly calculate significant quantities, like e.g. the hydrodynamic forces on a single grain, pressure-velocity-correlations, correlations between shear forces and coherent flow structures, etc. The long-term goal of these studies is to derive improved simple laws describing river bed stability. Such laws should enable a more reliable prediction of the stability of both natural beds and protection or flood defence works.

The tool used to realise the above mentioned velocity measurements is digital image processing. Optical 3-D methods based on digital image sequence analysis, like 3-D PTV or 3-D PIV, are well-known and widely used for quantitative visualisation of flow fields (e.g. Raffel et al., 1998). The presented setup is an implementation of a miniaturised, stereoscopic 3-D PTV system. Optical access to a single pore volume inside a gravel layer is given by flexible quartz fibre endoscopes (*bendoscopes*, see Figure 4). Image sequences are acquired, and the 3-D Lagrangian flow trajectories are determined from the image sequences by a 3-D PTV algorithm.

The paper is organised as follows. After this introduction, the experimental setup is described in detail in the next section. In the third section, the digital image processing techniques are briefly discussed. Some results are reported in the fourth section, and finally the work is summarised in the fifth section.



2. EXPERIMENTAL SETUP

2.1 The artificial pore, optical setup and visualisation

In order to measure the 3-D flow velocity inside a single pore of the gravel layer, a miniaturised stereo setup has been developed. The core of this setup is an artificial gravel pore, made of pebbles fixed to each other (see Figures 1, 5 and 8). This artificial pore defines the observation volume inside the gravel layer, resulting in a size of about 1 cm³. The mean diameter of the used grains is about 1 cm. Optical access to the artificial pore is given by two flexible fiber-optic endoscopes (Figure 4) viewing the pore volume from two different perspectives. The endoscopes have a diameter of about 2.4 mm. They are attached to a stereo rig consisting of two PVC spheres with drilled holes holding the endoscopes at a fixed position relative to each other. This stereo rig in turn is attached to the artificial pore. Before and after measurements, it can be taken off for calibration purposes without changing the relative position of the endoscopes.

Illumination of the measurement volume is provided by two additional fibre bundles, guiding the light from a halogen cold light source into the pore (Figure 6). A solution of polystyrol tracer particles of about 30 μm diameter is added to the pore flow upstream of the artificial pore in order to visualise the flow.

After a geometric calibration of the stereo rig has been performed, the pore is embedded into the gravel layer and flow measurements can be carried out. Particle image sequences of the two different endoscope views are recorded simultaneously by two standard monochrome CCD-cameras.

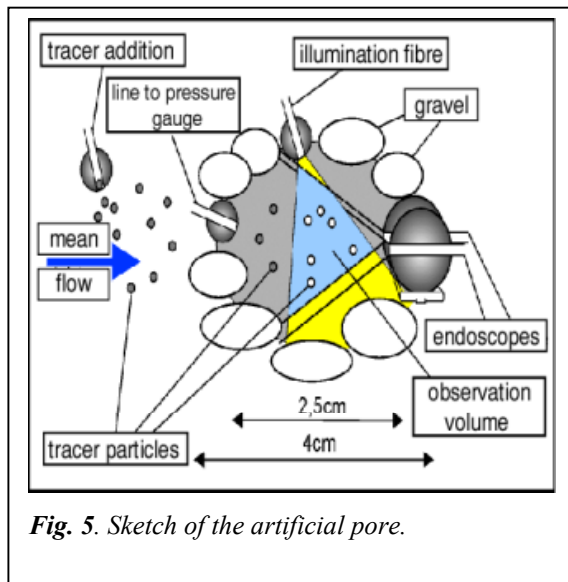


Fig. 5. Sketch of the artificial pore.

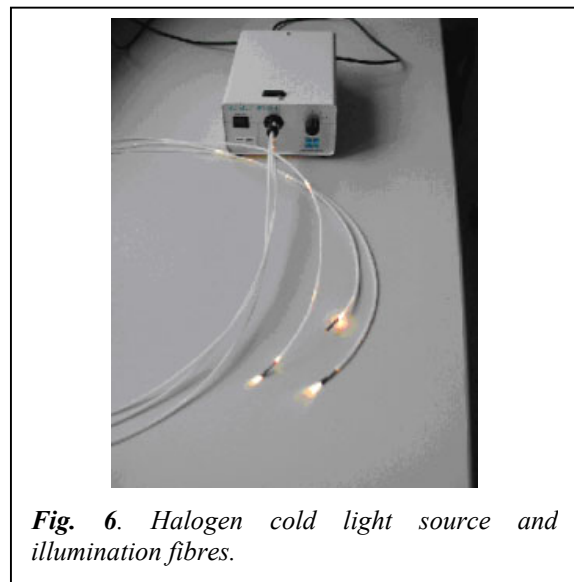


Fig. 6. Halogen cold light source and illumination fibres.

2.2 Data acquisition and computer hardware

Each endoscope is connected to a SONY XC-73CE CCD-camera, which provides 8 bit monochrome images with a resolution of 640x480 pixels at a frame rate of 25 Hz. The camera works in interlaced mode, i.e. each frame consists of two fields (even and odd image lines), which are exposed sequentially. To increase the temporal resolution (from 25 Hz to 50 Hz), each frame is decomposed into its two fields after acquisition of an image sequence. Due to this separation of even and odd fields, the height of the images is halved. To restore the original image size (and vertical resolution), the missing lines between the separated even/odd lines are interpolated.

A standard WindowsNT desktop PC is used to acquire and process the image data. The cameras are connected to a frame grabber card with two 8 bit input channels (ELTEC PCEye4). The frame grabber digitises the analogue camera signals and synchronises the stereo image acquisition. The memory size of 512 MB enables to capture a stereo sequence of 16 seconds duration. After recording a sequence, the image data is written to a RAID harddisk system for storage and further processing.

A second 3-D PTV system has been used to investigate the free surface flow straight above the gravel layer. Further, a third PC was used to acquire pressure data from five pressure gauges at different locations in and above the gravel layer. The three systems were operated simultaneously. The synchronisation was achieved by software triggering using a local network, i.e. no hardware triggering was used. Thus, the accuracy of the synchronisation was about 50 msec, which was sufficient for the present measurements.

2.3 The experimental flume and the considered experiments

Experiments have been conducted in a flume located at the Federal Waterways Engineering and Research Institute (Bundesanstalt für Wasserbau, BAW) in Karlsruhe, Germany. The flume is 40 m long, 1.1 m high and 0.9 m wide. A sand layer and a gravel filter layer have been deposited in the flume on a length of 20 m. The sand layer of 0.5 m height is covered by a gravel filter layer of 0.1 m height, see Figure 3. The grains in the gravel layer have a mean diameter of 10 mm. The measurement area is located 12 m downstream of the water inlet. Optical access is given by glass windows inserted into the channel walls on a length of 4 m. The endoscope setups and pressure gauges can be inserted into the gravel layer through holes in the glass windows, see Figure 7.

The flow discharge in the flume is controlled by an inductive flow meter, with a maximum flow rate of about 350 l/s. The water level in the flume can be adjusted by a movable weir at the channel outlet, the maximum water level is about 0.4 m, depending on the flow rate.



Fig. 7. View of the observation area from outside the channel.

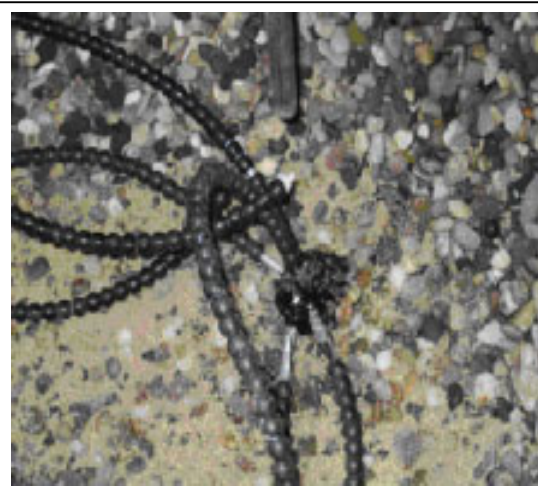


Fig. 8. Embedding the artificial pore at the bottom of the gravel layer.

Extensive pore flow measurements have been carried out in two experiments (I and II) under different flow conditions. The important parameters of the experiments and the hydrodynamic classification of the flows are compiled in table 1. In addition to the pore flow measurements, simultaneous 3-D PTV measurements of the free surface flow above the gravel layer have been done using another stereoscopic 3-D PTV setup (Klar, 2001). The shear velocities given in table 1 have been calculated from a fit of the logarithmic wall law to these data. Further, simultaneous measurements of pressure fluctuations at different locations of the flow field have been carried out by the Institute for Hydromechanics of the University of Karlsruhe.

Table 1. Flow parameters and classification.

Experiment	I	II	classification
flow discharge [l/s]	70.0	110.0	
water level [m]	0.4	0.4	
mean flow velocity [cm/s]	20.0	30.0	
total recording time [s]	990	1071	
number of image sequences	80	87	
images per sequence	742	742	
sequence length [s]	16	16	
Reynolds number (free surface flow)	66000	100000	fully turbulent
Froude number (free surface flow)	0.1	0.15	subcritical
roughness Reynolds number	133	192	completely rough
bed shear velocity [cm/s]	1.6	2.3	
bed shear stress [N/m ²]	0.3	0.5	stable bed
critical bed shear stress [N/m ²]	4.3	4.3	

The measurement procedure was the following: In order to measure a velocity profile throughout the gravel layer, the artificial pore had to be put in different vertical positions sequentially. First, it was deployed in the gravel layer at the lowermost position, i.e. at the top of the sand layer. The vertical position was measured by dropping a perpendicular on a marked grain of the artificial pore using a pointer gauge. The surface of the gravel layer was levelled, and water was supplied to the flume. After the desired water depth and stationary flow conditions had been achieved (which took approximately 30 minutes per run), the measurements were started. For each position of the artificial pore, ten image sequences have been recorded, each sequence of approximately 16 seconds length (corresponding to 512 MB RAM of the PC).

3. DIGITAL IMAGE PROCESSING

This section provides an overview of the basic principles of the 3-D PTV algorithm. In order to extract three-dimensional velocity vectors from the image data, a number of image processing steps are applied to the acquired image sequences, see the flowchart in Figure 9. The algorithm consists of several major components, which are discussed in the following subsections. The core of the algorithm is a stereo correlation of corresponding 2-D trajectories. Thus, in the first step, individual particles have to be identified in the images

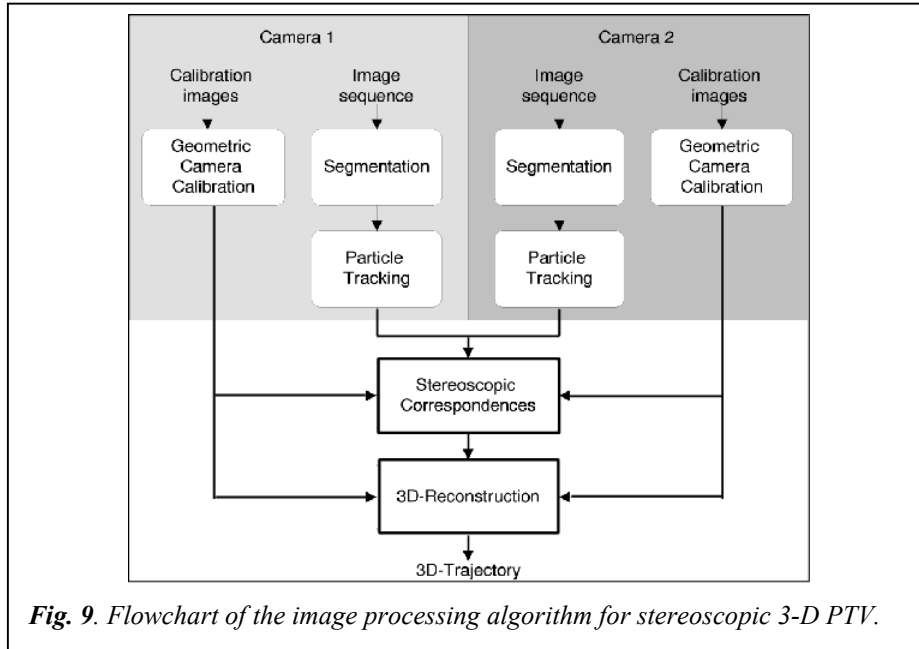


(image segmentation) and tracked from one frame to the next to build up 2-D trajectories (2-D PTV). After correspondences between such 2-D trajectories have been established, the world coordinates of the 3-D trajectories can be calculated by triangulation of the optical rays, provided that a geometric calibration of the two cameras has been performed before. This geometric calibration is discussed in the next subsection.

3.1 Geometric camera calibration

Camera model

In order to extract metric information from digital images, the relation between *image coordinates* (i.e. pixel positions in an image) and *world coordinates* (i.e. positions in 3-D space) has to be known. This relation is given by a camera model, a mathematical function \mathbf{F} describing the imaging process

$$\mathbf{x}=\mathbf{F}(\mathbf{X}),$$

where \mathbf{x} are the (2-D) image coordinates and \mathbf{X} are the (3-D) world coordinates. The camera is modelled by the well-known pinhole camera model, including correction terms for radial and tangential lens distortion (Tsai, 1987). The latter are of particular importance for the present application, since the endoscope optics introduces a significant amount of lens distortion to the images. Altogether, the camera model contains 15 camera parameters, which are estimated by the calibration algorithm: 6 external parameters (rotation, translation) and 9 internal parameters (effective focal length, aspect ratio, principal point and coefficients of radial and tangential distortion).

Calibration procedure

The calibration procedure is carried out according to a technique described in (Zhang, 2000). This technique only requires the camera to observe a planar calibration grid shown at several different orientations. Either the camera or the grid can be freely moved, and the relative motion need not be known. No expensive 3-D calibration targets are required. Both the internal and external camera parameters can be recovered from at least two different views of the calibration grid. To avoid modelling of multimedia transients (air-glas-water), the calibration of the endoscopes is performed in a vessel filled with water. Thus, a water proofed calibration grid has to be used, which is made by printing a grid pattern on a laser printer transparency and pasting the transparency on a small glass plate. The grid pattern is of size $2 \times 2 \text{ cm}^2$, and the grid spacing is 1 mm.

Feature extraction

Images of the calibration grid in a number of different orientations are acquired for both endoscopes in the stereo rig. The image coordinates of the grid points are extracted from the images using a subpixel-fit of a 2-D exponential function modelling the grayvalue distribution of intersecting grid lines (Garbe, 1998), see Figure 10. A precise determination of the image coordinates is complicated by the fibre-optic transmission of the images in the endoscopes. Images are transmitted by ordered fibres forming a hexagonal array. In every single fibre, the transmitted light intensity is maximum at the center of the fibre and drops to zero at the fringe, resulting in a honeycomb-like sampling of the image, see Figure 11. To reduce the influence of this honeycomb structure on the fit algorithm, the images are smoothed using a (2x2)-binomial filter mask.

Parameter estimation

Both the extrinsic and intrinsic camera parameters and the relative position and orientation of the calibration planes are estimated by the calibration algorithm. The procedure starts with a closed-form solution, which is followed by a nonlinear refinement using a least squares technique. The latter also includes the estimation of the distortion parameters. More details can be found in (Zhang, 2000).

The parameter estimation is first carried out separately for each of the two cameras. Since the positions and orientations of the calibration planes are the same for both cameras, the parameters of both cameras are re-estimated simultaneously in a further step, which yields a more precise parameter set for the stereo rig.

3.2 Particle tracking (2-D PTV)

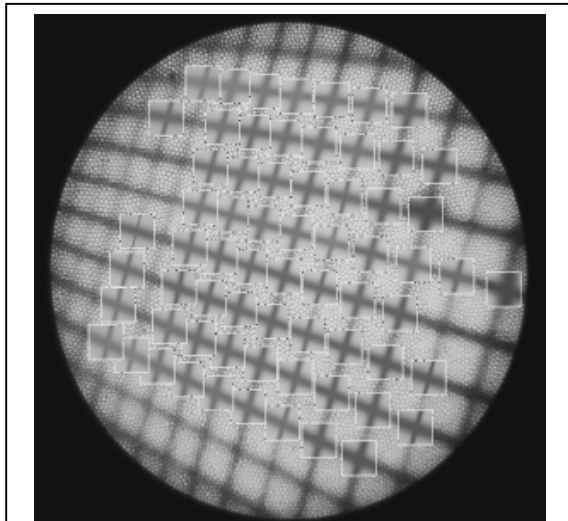


Fig. 10. Subpixel-fit of the grid line crossings. The result of the fit is plotted inside the boxes around the grid crossings.

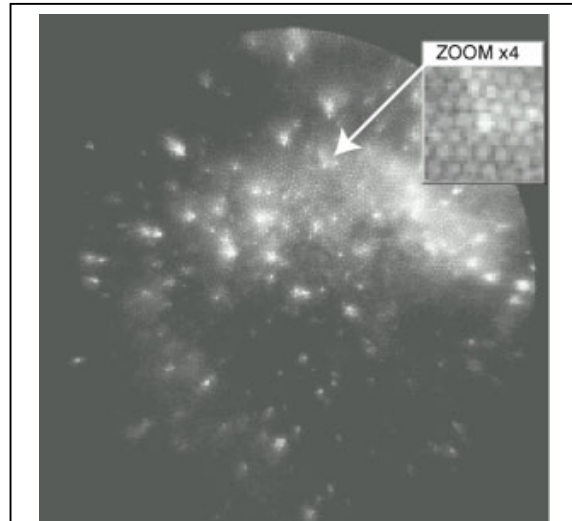


Fig. 11. Original endoscope image of tracer particles. The box shows a zoomed image area, the honeycomb-like structure is clearly visible.

Segmentation

The first step is to identify the particles in the images, i.e. to separate the pixels belonging to the particles from the image background (particle *segmentation*). This is one of the most crucial steps of the PTV algorithm, since segmentation failures result in broken, i.e. shorter 2-D trajectories. However, to reduce ambiguities in the 3-D reconstruction, the 2-D trajectories should be as long as possible.

To improve the image quality for the segmentation, different preprocessing steps are applied to the image sequences first. This includes a correction of inhomogeneous illumination by image normalisation, background subtraction and noise reduction by smoothing with a binomial filter. After these preprocessing steps, a simple greyvalue thresholding provided good segmentation results in most cases. However, in sequences with large velocity gradients which introduce very high greyvalue dynamics, more sophisticated segmentation algorithms have to be used, e.g. region-oriented or model-based methods (e.g. Hering et al., 1997).

Labelling

For the following image processing steps, the unique identification of each segmented particle is necessary. Thus, in the labelling step, all pixels belonging to the same particle are marked with a unique number; background pixels are marked with a zero. The resulting label image is used to calculate particle characteristics like area, greyvalue sum and center of mass.

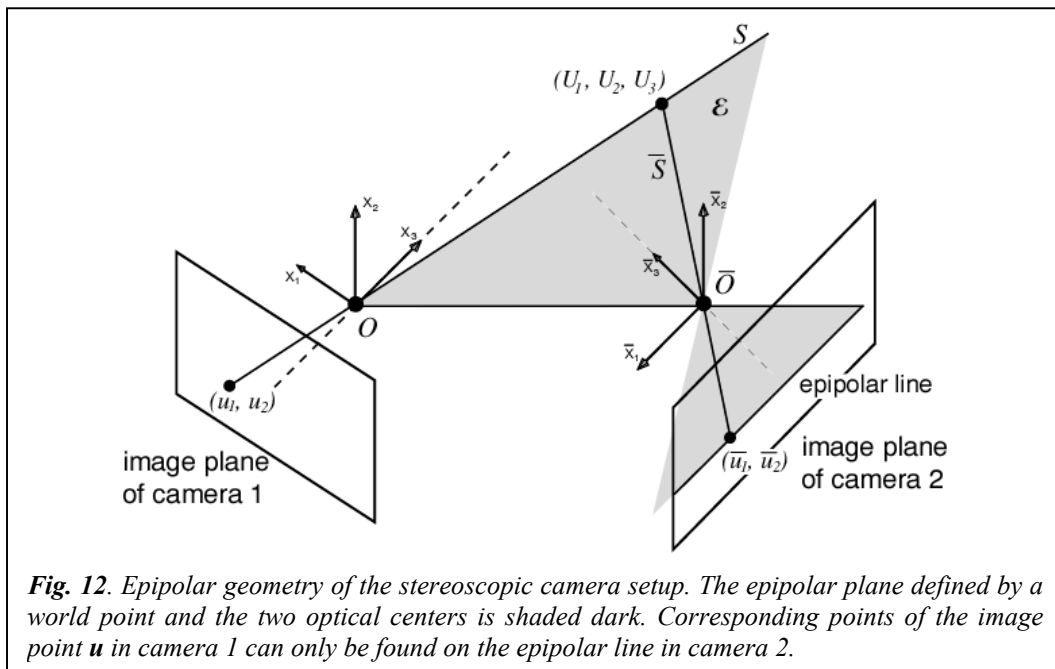
Tracking

To obtain the 2-D particle trajectories in the image plane, the correspondence problem of identifying the same particle in consecutive image frames has to be solved. Towards this end, each particle is enlarged individually by a morphological dilation operation. Particles in consecutive frames are marked as corresponding, if the dilated particle in frame i overlaps with its unique correspondence partner in frame $i+1$. However, the dilation operation is a sufficient criterion for the correspondence match only if the particle concentration remains smaller than about 100 particles per image. At higher particle concentrations, the probability of ambiguities due to the overlap of several possible correspondence partners increases. In this case, further particle information has to be used to solve the correspondence problem, e.g. area or greyvalue sum. In addition, information from the previous time steps along the particle's trajectory can be used, e.g. as input to a Kalman filter that calculates an estimate of the particle position and characteristics at the next time step.

3.3 Stereo correlation and 3-D coordinate calculation

To enable the reconstruction of the 3-D particle positions, the stereo correspondence problem has to be solved, i.e. corresponding particle images have to be identified uniquely in the stereoscopic views. The correspondence can be established using the constraint imposed by the epipolar geometry of the stereoscopic setup (Xu and Zhang, 1996): a correspondence partner of a particle in the left image can only be found on its epipolar line in the right image. However, because particle images cannot be distinguished by individual object properties, the correspondence search is rendered more difficult because of ambiguities: in most cases several possible corresponding particle images can be found on the epipolar line, i.e. several particles in one image are located in the epipolar plane in 3-D space, see Figure 12. The number of ambiguities can be significantly reduced by considering particle trajectories, i.e. lists of temporally subsequent particle images, instead of single particle images in the correspondence search. For a unique correlation, the epipolar constraint is imposed on all particle images forming a trajectory rather than on a single particle image. Particle trajectories can be distinguished from each other more easily, and the additional information of the geometric shape of the trajectory, which is not available in the case of matching single particles, can be used to reduce ambiguities (e.g. Engelmann et al., 1998).

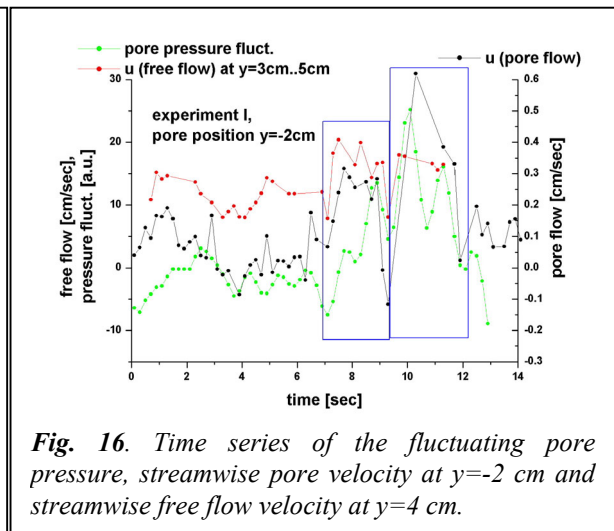
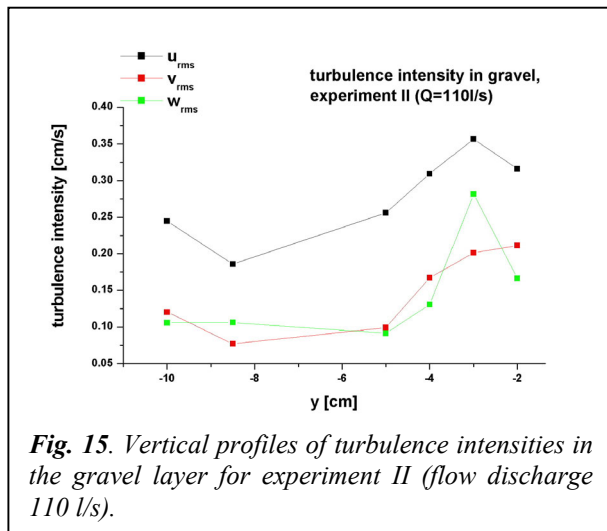
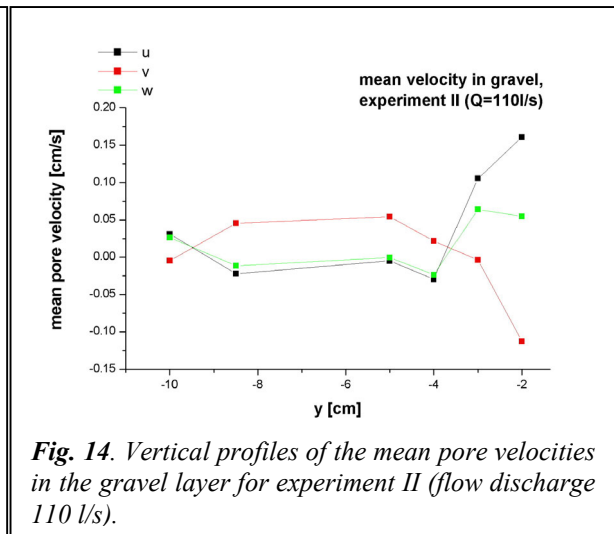
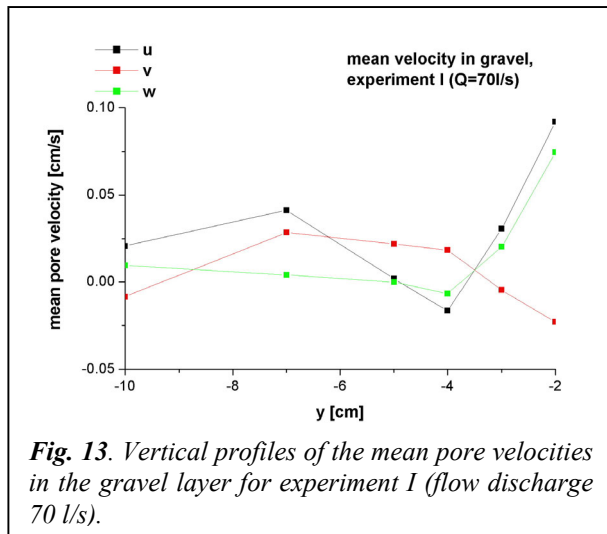
Once a unique correspondence between two 2-D trajectories has been established, the 3-D world coordinates are



readily calculated by triangulation. A first order estimate of the particle velocity is then given by the 3-D distance of subsequent particle positions and the frame rate of the camera.

4. RESULTS AND DISCUSSION

In this section, some results of the experiments described in section 2.3 are reported and discussed. Figures 13 and 14 show the mean velocity profiles in the gravel layer as a function of the vertical coordinate y for experiments I and II. The mean flow velocities are obtained by temporal averaging over all image sequences acquired for one pore position and spatial averaging over the pore volume. They are denoted by u , v and w in streamwise, vertical and spanwise direction respectively. The sand/gravel-boundary is at $y=-10$ cm, the free surface flow is in the area of positive y -values. Both plots show a relatively large velocity gradient in the upper grain layers, reflecting the strong impact of the turbulent free surface flow on the pore flow. The turbulence intensity in the gravel layer is also decreasing from the top to the bottom of the gravel layer, see Figure 15. Comparable results have been reported in (Shimizu et al., 1990). Further, the pressure fluctuations measured simultaneously in the present experiments are dampened in a similar way towards the bottom of the gravel layer (Lang et al., 2001). The results indicate the interaction of the free surface flow and the pore flow, i.e. the exchange of mass and momentum between the two flows. The pore flow, in particular in the upper grain layers, is governed by the free surface flow near the bed, which in turn affects quantities like the flow discharge or sediment discharge inside the gravel layer. At the same time, the structure of the free surface flow near the bed is



altered by the presence of the porous medium at the bottom wall, compare the discussion below.

For experiment I, the streamwise mean filter velocity inside the gravel layer calculated from the profile in Figure 13 is about 0.03 cm/sec. A comparable value of 0.045 cm/sec follows from a calculation using Darcy's law. However, the latter value has to be considered as a crude approximation, since the boundary conditions that are necessary for the application of Darcy's law are not given due to the interaction with the free surface flow as just mentioned. The pore flow Reynolds number calculated from the mean filter velocity and the mean grain diameter is about 1.0, indicating that the pore flow is rather in a laminar/transitional than in a fully turbulent state. This is also confirmed by visual inspection of the image sequences. Turbulent fluctuations mainly take place in single, intermittent events.

The mean velocity profiles show that there is a trend for the vertical velocity to become negative towards the boundary to the free surface flow. This means, that in the mean flow, fluid is penetrating from the free surface flow into the pore flow. Of course, these results don't represent the overall, global flow behaviour in the gravel bed, but only the local flow in the artificial pore. However, such behaviour is in agreement with recent results reported in (Dancey et al., 2000). These authors found, that the mean vertical velocities directly above an artificial porous bed made of glass beads were mainly directed into the bed, while the mass and momentum fluxes out of the bed take place in turbulent fluctuations and are confined to single spots between the glass beads. Similar jet-like ejections of pore fluid into the free surface flow have been visualised in our experiments, see Figures 17 and 18. These ejections also took place intermittently at single locations of the bed, with a period of about 2-3 seconds.

Time series of the pore velocities have been calculated by averaging over 10 frames, yielding a temporal resolution of 0.2 sec. Again, spatial averaging over the pore volume has been carried out. The length of the time



Fig. 17. Jet-like fluid ejection from the pore flow into the free surface flow, $t=0$ sec. The top of the gravel layer can be seen at the bottom of the image, the mean flow is from left to right.



Fig. 18. Jet-like fluid ejection from the pore flow into the free surface flow, $t=0.5$ sec. The ejection is visualised by the pore flow tracer solution. Ejections like this take place with a period of about 2-3 sec

series is limited by the image sequence duration of about 16 seconds for the pore flow and 12 seconds for the free surface flow. An example of the resulting time series is shown in Figure 16. In this figure, the instantaneous pore pressure, the streamwise pore velocity at $y=-2$ cm and the streamwise free flow velocity at $y=4$ cm are plotted. The latter has been calculated by averaging the free surface flow PTV data over a horizontal layer of 2 cm height. A correlation of the velocity and pressure fluctuations can be made out clearly, indicated by the blue boxes. Large fluctuations of the considered quantities take place simultaneously, revealing the penetration of turbulent fluctuations from the free surface flow into the gravel bed. In similar time series plots like the one in Figure 16, a clear periodicity of the correlated pressure and velocity fluctuations has been found (Klar, 2001, Stybalkowski, 2001). This periodicity indicates, that the fluctuations may be dominated by surface waves in the open-channel flow. Indeed, the results of (Lang et al., 2001) show that the pressure fluctuations in the gravel layer mainly reflect the fluctuations of the water level, which have also been measured using an ultrasonic probe. Interestingly, the fluctuations of the water level are of the order of magnitude of only 1 mm, but the wave periods can still be seen in the velocity fluctuations in the deepest grain layers at the bottom of the gravel bed ($y=-10$ cm).

5. CONCLUSION AND OUTLOOK

A novel experimental setup enabling miniaturised 3-D PTV measurements within a gravel layer has been presented. Optical access to a single gravel pore is given by flexible quartz-fibre endoscopes in a stereo setup and fibre-optic illumination. 3-D Lagrangian flow fields are calculated from the acquired image sequences using digital image processing techniques, stereo correlation and triangulation. Correlating 2-D trajectories instead of the positions of single particles allows for a simple setup with a minimum number of two cameras resp. endoscopes. It could be shown that the present setup is well-suited for the measurement of pore velocities inside a single pore volume of a gravel layer. Experimental results from an open-channel flow above a gravel bed have been reported. Profiles of mean pore velocity and turbulence intensity clearly show the impact of the turbulent free surface flow on the pore flow, in particular in the upper grain layers. The results are in good agreement with

previous results reported in the literature. Further, the results of the velocity estimates have been verified by simultaneous pressure measurements.

Future work includes a further miniaturisation of the artificial pore volume, simultaneous measurements in three artificial pores at different locations in the gravel layer, unstationary flow conditions (large surface waves) and additional observation of incipient sediment transport at the sand-gravel interface using rigid endoscopes.

ACKNOWLEDGEMENTS

Financial support provided by the BAW Karlsruhe is gratefully acknowledged. In particular, the authors would like to thank Dipl.-Ing. H.-J. Köhler and Dr. Thomas Wenka for initiating and maintaining the long standing cooperation with the IWR. Further, we would like to thank Helge Daebel, Francisco de los Santos Ramos and Gregor Kühn of the Institute for Hydromechanics (Prof. G. H. Jirka) of the University of Karlsruhe for the close and fruitful cooperation during preparation, implementation and evaluation of the measurements and for providing the pressure data.

REFERENCES

- Clifford, N. J., French, J. R. and Hardisty, J. (eds.) (1993). "Turbulence. Perspectives on Flow and Sediment Transport", John Wiley & Sons, Chichester.
- Dancey, C. L., Balakrishnan, M., Diplas, P. and Papanicolaou, A. N. (2000). "The spatial inhomogeneity of turbulence above a fully rough, packed bed in open channel flow", *Experiments in Fluids*, 29, pp. 402-410.
- Dey, S., Dey Sarker, H. K., and Debnath, K. (1999). "Sediment Threshold under Stream Flow on Horizontal and Sloping Beds", *Journal of Engineering Mechanics*, 125, (5), pp.545-553.
- Dittrich, A. (1997). "Wechselwirkung Morphologie/Strömung naturnaher Fließgewässer", Professorial Dissertation, University of Karlsruhe, Germany.
- Dittrich, A., Nestmann, F. and Ergenzinger, P. (1996). "Ratio of Lift and Shear Forces Over Rough Surfaces". In: Coherent Flow Structures in Open Channels, ed. Ashworth et al., John Wiley & Sons, pp. 125-146.
- Engelmann, D., Garbe, C., Stoehr, M., Geissler, P., Hering, F. and Jaehne, B. (1998). "Stereo Particle Tracking", *Proceedings of the 8th International Symposium on Flow Visualization*, Sorrento, Italy.
- Garbe, C. (1998). "Entwicklung eines Systems zur dreidimensionalen Particle Tracking Velocimetry mit Genauigkeitsuntersuchungen und Anwendung bei Messungen in einem Wind-Wellen Kanal", Diploma Thesis, University of Heidelberg. Available at <http://klimt.iwr.uni-heidelberg.de>.
- Garcia, M., Lopez, F. and Nino, Y. (1995). "Characterization of near-bed coherent structures in turbulent open channel flow using synchronized high-speed video and hot-film measurements", *Experiments in Fluids*, 19, pp. 16-28.
- Grass, A. J. (1971). "Structural features of turbulent flow over smooth and rough boundaries", *Journal of Fluid Mechanics*, 50, pp. 233-255.
- Grass, A. J., Stuart, R. J. and Mansour-Tehrani, M. (1991). "Vortical structures and coherent motion in turbulent flow over smooth and rough boundaries", *Phil. Trans. R. Soc. Lond. A*, 336, pp. 35-65.
- Hering, F., Wierzimok, D., Leue, C. and Jaehne, B. (1997). "Particle tracking velocimetry beneath water waves. Part I: visualization and tracking algorithms.", *Experiments in Fluids*, 23, (6), pp. 472-482.
- Klar, M. (2001). "3-D Particle-Tracking Velocimetry applied to Turbulent Open-Channel Flow over a Gravel Layer", Diploma Thesis, University of Heidelberg. Available at <http://klimt.iwr.uni-heidelberg.de>.
- Kline, S. J., Reynolds, W. C., Schraub, F. A. and Runstadler, P. W. (1967). "The structure of turbulent boundary layers", *Journal of Fluid Mechanics*, 30, pp. 741-773.
- Lang, C., de los Santos Ramos, F. J., Kühn, G. (2001). "Untersuchungen zur Stabilität poröser Gerinnesohlen", Report Nr. 782 of the Institute for Hydromechanics, University of Karlsruhe.

- Nezu, I. and Nakagawa, H. (1993). "Turbulence in Open-Channel Flows", IAHR/AIRH Monograph Series, Balkema Publishers, Rotterdam.
- Pye, K. (ed.) (1994). "Sediment Transport and Depositional Processes", Blackwell Scientific Publications, Oxford.
- Raffel, M., Willert, C., and Kompenhans, J. (1998). "Particle Image Velocimetry", Springer, Heidelberg.
- Sechet, P. and Le Guennec, B. (1999). "Bursting phenomenon and incipient motion of solid particles in bed-load transport", *Journal of Hydraulic Research*, 37, (5), pp. 683-696.
- Shields, A. (1936). "Anwendung der Ähnlichkeitsmechanik und der Turbulenzforschung auf die Geschiebebewegung", *Mitteilungen der Preußischen Versuchsanstalt für Wasserbau und Schiffbau*, 26, pp. 5-24. Berlin.
- Shimizu, Y., Tsujimoto, T. and Nakagawa, H. (1990). "Experiment and macroscopic modelling of flow in highly permeable porous medium under free-surface flow", *Journal of Hydrosience and Hydraulic Engineering*, 8, (1), pp. 69-78.
- Stybalkowski, P. (2001). "Strömungsmessung in Sedimentporen mittels 3-D Particle Tracking Velocimetry", Diploma Thesis, University of Heidelberg. Available at <http://klimt.iwr.uni-heidelberg.de>.
- Thorne, C. R., Bathurst, J. C. and Hey, R. D. (eds.) (1987). "Sediment Transport in Gravel-Bed Rivers", John Wiley & Sons, Chichester.
- Tsai, R. Y. (1987). "A versatile camera calibration technique for high-accuracy 3D machine vision metrology using off-the-shelf tv cameras and lenses", *IEEE Journal of Robotics and Automation*, 3, (4), pp. 323-344.
- Xu, G. and Zhang, Z. (1996). "Epipolar Geometry in Stereo, Motion and Object Recognition", Kluwer Academic Publishers, Dordrecht, The Netherlands.
- Yalin, M. S. (1977). "Mechanics of sediment transport (2nd ed.)", Pergamon Press, Oxford.
- Yalin, M. S. (1992). "River Mechanics", Pergamon Press, Oxford.
- Zhang, Z. (2000). "A flexible new technique for camera calibration", *IEEE Transactions on Pattern Analysis and Machine Intelligence*, 22, (11), pp. 1330-1334.